Inorganica Chimica Acta 425 (2015) 76–82

Contents lists available at ScienceDirect

Inorganica Chimica Acta

journal homepage: www.elsevier.com/locate/ica

A comparison of charge-transfer mechanisms at rotated disk electrode for biomimetic binuclear and tetranuclear oxo-manganese complex in aqueous solution

Cibely S. Martin, Marcos F.S. Teixeira *

Faculty of Science and Technology, São Paulo State University (UNESP), Rua Roberto Simonsen, 305, CEP 19060-900 Presidente Prudente, SP, Brazil

ARTICLE INFO

Article history:
Received 3 June 2014
Received in revised form 10 October 2014
Accepted 12 October 2014
Available online 29 October 2014

Keywords:
Biomimetic
Oxo-manganese complexes
Rotating disk electrode
Change transfer mechanism
Tafel behavior

ABSTRACT

Many high-valence multinuclear μ-oxo-bridged manganese complexes have been synthesized to mimic the active site of the natural enzymes. The electrochemical and kinetic parameters were determined for two *mimicking* complexes ($[Mn_2^{IV}O_2(terpy)_2(H_2O)_2]^{4+}$ and $[Mn_4^{IV}O_5(terpy)_4(H_2O)_2]^{6+}$) by cyclic voltammetry and linear sweep voltammetry using a rotating disk electrode (RDE). Stability and kinetic behavior are directly related to μ-oxo bridges, where the μ-oxo-bridge provides a fast electron transition between metal centers due to stabilization of $dx^2 - y^2$ orbitals by the oxygen bond. On the other hand, when the $dx^2 - y^2$ orbitals are stabilized by *aqua* ligands by a coordination bond, a displacement of oxidation potential to more positive potential was observed. A shift of the potential to more negative values with increase in rotation rate was observed, which can be ascribed to a chemical step. The chemical step involves the dimerization process of the binuclear oxo-manganese complex to tetranuclear oxo-manganeses complex.

1. Introduction

The μ-oxo-bridged manganese complexes has been widely investigated as biomimetic molecules of active enzymes sites and applied in both homogeneous and heterogeneous catalysis [1–6]. The strategy of using different ligands in complex synthesis has helped in understating the structure/function of the manganese ions in many modeling of metalloproteins and elucidating the performance of this metal ion in enzymes. The importance of this kind of complex in biological areas has generated several complexes, which are currently used as catalysts and electrocatalysts for the oxidation of both organic compounds [7–12] and water [13,14]. Among the numerous polynuclear complexes with μ-oxo bridges that have been prepared as possible models of the active site of photosystem II [15], only cationic species such as $[Mn_2^{III,IV}O_2(bpy)_4]^{3+}$ (bpy = 2,2′-bipyridine) and the analogues of the 1,10-phenantroline complex have been reported to be active to O_2 evolution from water oxidation [16]. However, studies show that $[Mn_2^{III,IV}O_2(bpy)_4]^{3+}$ species are unstable in aqueous solution no buffered, forming the $[Mn_4^{IV}O_6(bpy)_6]^{4+}$ species, which is stable in aqueous solution, but inactive as an O_2 catalyzer [17,18]. Some studies show that complexes with tridentate ligand, such as dipicolinate (dpa) or 2,2′:6′,2″-terpyridine (terpy), are able to induce O_2 evolution, where the terpyridine complexes show higher stability in aqueous solution, ascribed to coordination with aqua ligand [5]. On the other hand, recently the Najafpour et al. [19] showed that $[Mn_2^{III,IV}O_2(terpy)_2(H_2O)_2]^{3+}$ is not active catalyst for water, but this species are transformed into layered type Mn-oxide particles (formed by the Ce(IV) oxidant), which are the actual water oxidation catalyst. This effect was also proposed and described in the literature by other researchers [20]. However this question remains open, and more studies with these complexes are important.

In the literature mechanistic hypotheses based on studies of biomimetic compounds have been developed [21–23] and several types of manganese model complexes with enzymatic activity have been reported [16,24–26]. The Baffert et al., described a stability studies of $[Mn_2^{III,IV}O_2(terpy)_2(H_2O)_2]^{3+}$ complex in aqueous solution, where demonstrated that this complex undergoes a quite rapid evolution to the $[Mn_4^{IV}O_5(terpy)_4(H_2O)_2]^{6+}$ complex, having a linear mono-μ-oxo-$\{Mn_2(\mu\text{-oxo})_2\}_2$ core [1]. These complexes show a distorted octahedral geometry at each manganese center, where the coordination spheres consist of three N atoms from a single terpy ligand and di-μ-oxo bridge and for the tetranuclear complex, one μ-oxo-bridge links the binuclear unities. Besides, two *aqua* ligand is coordinated in *trans* orientation at the end of complex (Mn-O_{aqua} bond) [1–3]. This way, kinetic studies is of great importance to available the charge-transfer mechanisms in

* Corresponding author. Tel.: +55 18 32295355; fax: +55 18 32215682.
E-mail address: funcao@fct.unesp.br (M.F.S. Teixeira).

http://dx.doi.org/10.1016/j.ica.2014.10.009
0020-1693/

biomimetic structures and understands the dimerization process. Here, we report the syntheses and electrochemical properties of the new complexes $[Mn_2^{IV,IV}O_2(terpy)_2(H_2O)_2]^{4+}$ and $[Mn_4^{IV}O_5(terpy)_4(H_2O)_2]^{6+}$, where the charge-transfer mechanism using a rotating disk electrode was proposed.

2. Experimental

2.1. Reagents and solution

The $[Mn_2^{IV}O_2(terpy)_2(H_2O)_2]^{4+}$ (binuclear oxo-manganese complex) and $[Mn_4^{IV}O_5(terpy)_4(H_2O)_2]^{6+}$ (tetranuclear oxo-manganese complex) were synthesized according to the procedure adapted from literature [2,3]. All chemicals were analytical reagent grade and were used without further purification. The supporting electrolyte used for all experiments was a 0.5 mol L^{-1} $NaNO_3$ solution. A ~1.0 mmol L^{-1} complex solution was prepared in 25.0 mL of $NaNO_3$ solution (0.5 mol L^{-1}).

2.2. Synthesis of $[Mn_2^{IV}O_2(terpy)_2(H_2O)_2]^{4+}$

The $[Mn_2^{IV}O_2(terpy)_2(H_2O)_2](NO_3)_4{\cdot}6H_2O$ complex was synthesized according to adaptations of the literature procedure [3]. 2,2′:6,2″-Terpyridine (Fluka) (0.72 mmol) was dissolved in acetone (Synth), in which $Mn(NO_3)_2{\cdot}4H_2O$ (Aldrich) (0.48 mmol) in H_2O was added. After all reactants were dissolved, the yellow mixture was stirred in an ice bath for 15 min. Then, the $KMnO_4$ (1.3 mmol – Aldrich) in water was added dropwise to the mixture, which turned deep green in about 15 min. The mixture was kept in stirring for 30 min, after was cooled at 5 °C for 24 h. The solids were carefully separated and washed with several drops water. The final product was left in desiccators for complete evaporation of the solvent. Is important to note that adaptations of the synthesis procedure allowed obtain the $[Mn_2^{IV}O_2(terpy)_2(H_2O)_2]^{4+}$ species, which was confirmed by the electrochemical measurements.

2.3. Synthesis of $[Mn_4^{IV}O_5(terpy)_4(H_2O)_2]^{6+}$

The $[Mn_4^{IV}O_5(terpy)_4(H_2O)_2](ClO_4)_6{\cdot}3H_2O$ complex was synthesized according to the procedure of literature [2]. 2,2′:6,2″-Terpyridine (Aldrich) (0.63 mmol) was dissolved in CH_3CN, in which $Mn(NO_3)_2{\cdot}4H_2O$ (Aldrich) (0.60 mmol) in H_2O was added. After all reactants were dissolved, the yellow mixture was stirred in an ice bath for 10 min. Then the Oxone® (0.90 mmol – Aldrich) in water was added dropwise to the mixture, which turned deep red in about 15 min. A large excess of solid $NaClO_4$ was added to the mixture, and the pH of the solution was adjusted to 2 by addition of concentrated HNO_3. This mixture was transferred to a series of small test tubes and allowed to slowly evaporate in the dark. As a result, needle-like black-red crystals of $[Mn_4^{IV}O_5(terpy)_4(H_2O)_2](ClO_4)_6$ and orange-red crystals of $[Mn^{II}(terpy)_2](ClO_4)_2$ were formed concomitantly in approximately two weeks. The needles were carefully separated and washed first with several drops of HNO_3 solution (pH 2) and then with 3 mL of diethyl ether. The final product was left in desiccators for complete evaporation of the solvent.

2.4. Apparatus

All voltammetric measurements were carried out in a 25 mL thermostatic glass cell containing three electrodes: a glassy carbon electrode as the working electrode (surface area 0.072 cm^2), a saturated calomel electrode (SCE) as the reference, and a platinum wire as auxiliary electrode. Prior to use, the working electrode was immersed in a solution of H_2SO_4 and H_2O_2 30% (3:1), polished with an aqueous solution suspension of 0.05 μm alumina slurry, washed with ethanol, and then rinsed with deionized water.

2.5. Electrochemical measurements

The electrochemical behavior in aqueous solution and kinetic parameters were determined by cyclic voltammetry (CV) and linear sweep voltammetry with a rotating disk electrode (RDE), respectively. The measurements by cyclic voltammetry were performed in a range potential of 0.2–1.2 V versus SCE at a scan rate of 25 mV s^{-1}. The measurements by RDE were performed in a range potential of 0.2–1.0 V versus SCE at a scan rate of 25 mV s^{-1} in a range of rotation rate of 100 to 5000 rpm. The electrochemical measurements were carried out using 0.5 mol L^{-1} $NaNO_3$ solutions containing the maximum concentration of the respective complex (~1.0 mmol L^{-1}). All electrochemical measurements were performed with a μ-AUTOLAB type III (Eco Chimie) controlled by a computer. In addition, for RDE study was used the AUTOLAB RDE that consist of the mechanical unit (RDE-2) connecting to motor control unit (MCUR).

3. Results and discussion

3.1. Electrochemical behavior by cyclic voltammetry

The electrochemical characterization of $[Mn_2^{IV}O_2(terpy)_2(H_2O)_2]^{4+}$ (binuclear oxo-manganese complex) and $[Mn_4^{IV}O_5(terpy)_4(H_2O)_2]^{6+}$ (tetranuclear oxo-manganese complex) by cyclic voltammetry was performed using 0.5 mol L^{-1} $NaNO_3$ (pH 4.7) as supporting electrolyte at a scan rate of 25 mV s^{-1}. The cyclic voltammograms (Fig. 1) performed in a range potential of 0.2–1.2 V versus SCE show one redox couple with half-wave potential of $E_{p/2}$ = 0.76 V versus SCE for binuclear complex and

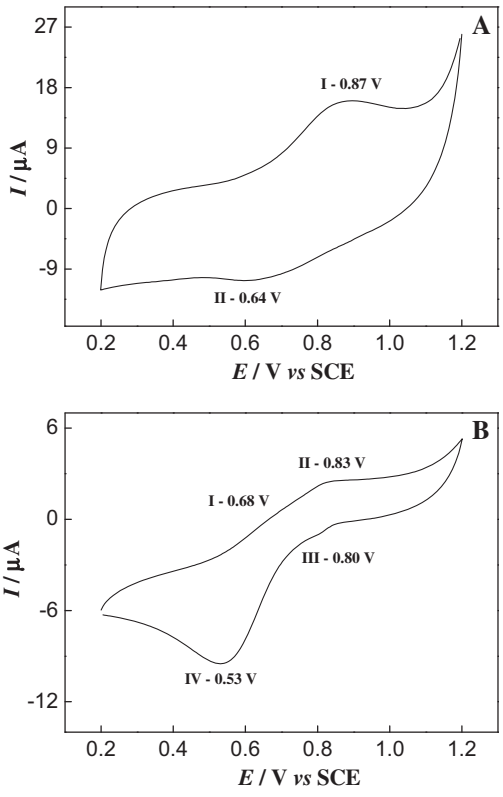

Fig. 1. Voltammetric profiles of (A) binuclear oxo-manganese complex and (B) tetranuclear oxo-manganese complex in 0.5 mol L^{-1} $NaNO_3$ (pH 4.7) at 25 mV s^{-1}.

two redox couple with a half-wave potential of $E_{p/2}$ = 0.60 V and 0.82 V versus SCE for tetranuclear complex, where $E_{p/2}$ = $(E_{pa} + E_{pc})/2$.

The redox process observed for binuclear oxo-manganese complex ($E_{p/2}$ = 0.76 V versus SCE) can be ascribed to the $Mn^{(IV)}O_2Mn^{(III)}/Mn^{(IV)}O_2Mn^{(IV)}$ redox couple (Scheme 1). However, for tetranuclear oxo-manganese complex, the redox process I/IV ($E_{p/2}$ = 0.60 V versus SCE) can be ascribed to $Mn^{(IV)}O_2Mn^{(III)}OMn^{(III)}O_2Mn^{(IV)}/Mn^{(IV)}O_2Mn^{(IV)}OMn^{(IV)}O_2Mn^{(IV)}$ redox couple (Scheme 1), while the redox process II/III ($E_{p/2}$ = 0.82 V versus SCE) can be ascribed to the $Mn^{(IV)}O_2Mn^{(III)}/Mn^{(IV)}O_2Mn^{(IV)}$ redox couple, which is similar to observed for binuclear complex. This behavior suggests a possible equilibrium between binuclear oxo-manganese and tetranuclear oxo-manganese complex in solution.

In addition, the current magnitude of the cathodic peak in 0.53 V (reduction of Mn^{IV} to Mn^{III}) observed to tetranuclear complex was higher than of other peaks, that can be related to Jahn Teller effect. This way, the reduction of Mn^{IV} to Mn^{III} could be more favorable between mono-μ-oxo bridges due to $dx^2 - y^2$ orbitals, available for electron transition between Fermi level of the electrode and the orbital *d* of metal, which minimizes the *Jahn Teller* effect.

For better observation of the redox process, more measurements using differential pulse voltammetry were performed. The differential pulse voltammograms (Fig. 2) were obtained under the same conditions as cyclic voltammetry using a pulse of 100 mV for tetranuclear oxo-manganese complex in positive sweep and negative sweep. The redox potential observed in differential pulse voltammetry was displaced to a more positive potential in relation to cyclic voltammetry due to the pulse utilized. For tetranuclear complex, the process observed with $E_{p/2}$ = 0.915 V versus SCE can be ascribed to the $Mn^{(IV)}O_2Mn^{(III)}/Mn^{(IV)}O_2Mn^{(IV)}$ redox couple. Therefore, the redox couple in $E_{p/2}$ = 0.765 V versus SCE can be ascribed to $Mn^{(IV)}O_2Mn^{(III)}OMn^{(III)}O_2Mn^{(IV)}/Mn^{(IV)}O_2Mn^{(IV)}OMn^{(IV)}O_2Mn^{(IV)}$, having a linear mono-$\mu$-oxo-$\{Mn_2(\mu\text{-oxo})_2\}_2$ core. The redox couple of high potential (E_{pa} = 0.96 V and E_{pc} = 0.87 V versus SCE) indicates the presence of a binuclear complex with a di-μ-oxo-bridge [1,2,18,27,28].

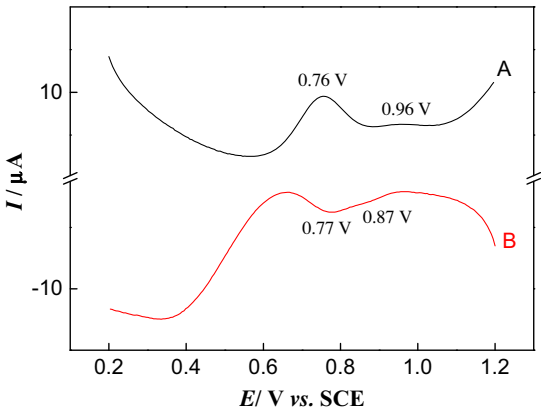

Fig. 2. Differential pulse voltammograms recorded as a positive sweep (A) and as a negative sweep (B) for tetranuclear oxo-manganese complex at 25 mV s^{-1}. Pulse at 100 mV.

The differential pulse voltammograms recorded to tetranuclear oxo-manganese complex, showed high peak current to first redox process, which can be ascribed to high concentration of the tetranuclear species than binuclear species in solution. Moreover, the presence of the second potential peak with low peak current ascribed to binuclear species suggests equilibrium between both species through of the dimerization process. The tetranuclear oxo-manganese complex can be formed by a dimerization process from the binuclear oxo-manganese complex, where the μ-oxo-bridge results from deprotonation of one *aqua* ligand (Scheme 2), which involves the $dx^2 - y^2$ orbitals of manganese centers [1,29]. In aqueous solution, the stability of binuclear complex can be ascribed to fast evolution of the tetranuclear species [1,2,29]. When comparing the voltammetric profiles of the binuclear and

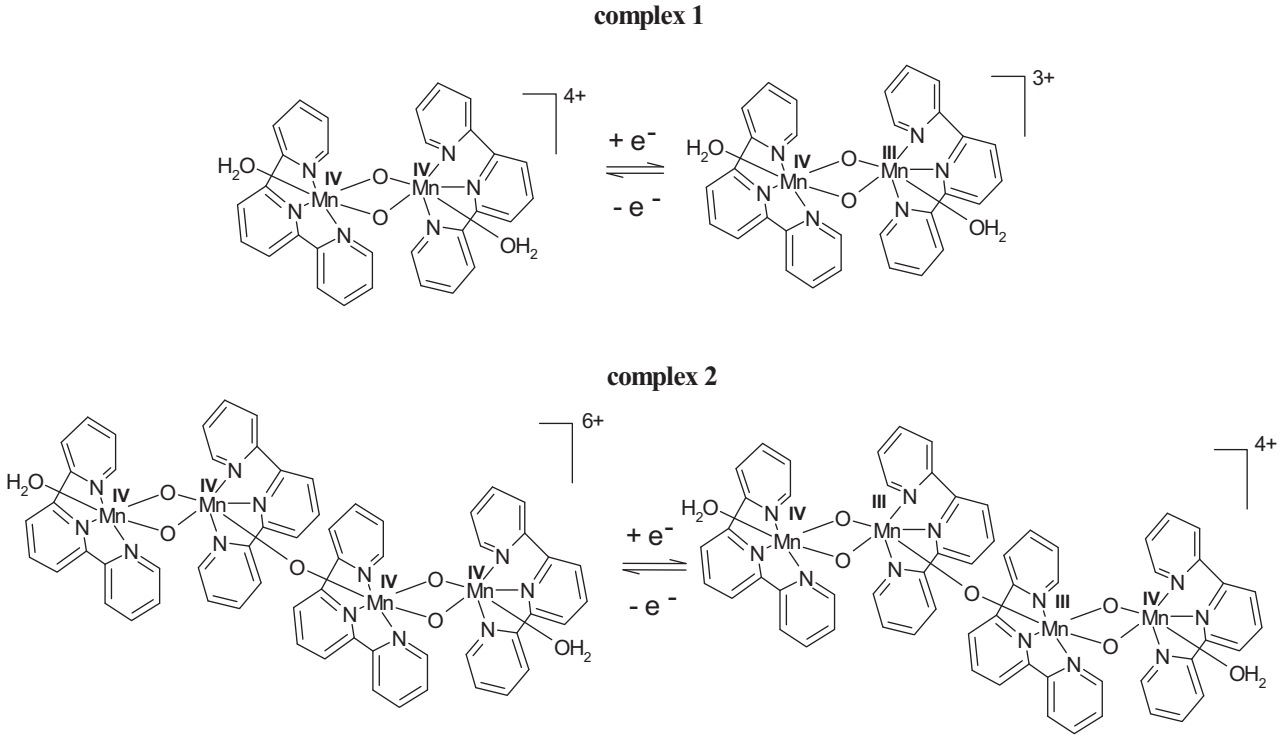

Scheme 1. Representation of electrochemical process of the $Mn^{(IV)}O_2Mn^{(IV)}$ to $Mn^{(IV)}O_2Mn^{(III)}$ for binuclear complex (**1**) and $Mn^{(IV)}O_2Mn^{(IV)}OMn^{(IV)}O_2Mn^{(IV)}$ to $Mn^{(IV)}O_2Mn^{(III)}OMn^{(III)}O_2Mn^{(IV)}$ for tetranuclear complex (**2**).

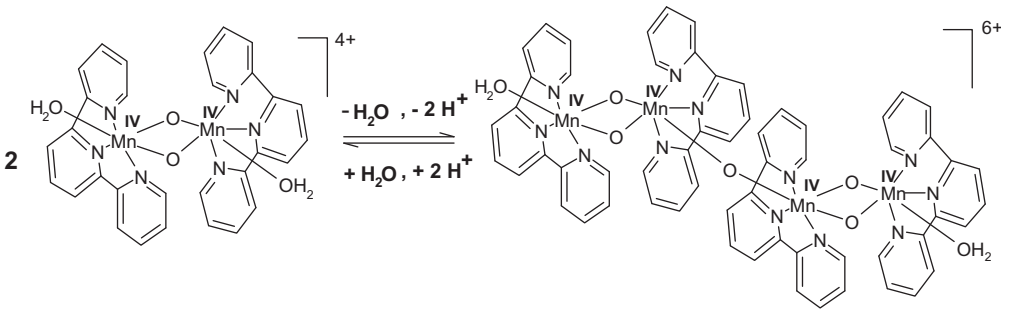

Scheme 2. Interconversion of binuclear to tetranuclear oxo-manganese complexes in aqueous solution [1]. Chemical step.

tetranuclear (Fig. 1), there is a displacement of the potential to a more negative value for tetranuclear oxo-manganese complex, which can be ascribed to the higher stability of cluster structure due to μ-oxo bridge formation between the dimers with a di-μ-oxo bridge [29]. This displacement can also be ascribed to overlap of two redox processes to tetranuclear oxo-manganese complex.

3.2. Kinetics parameters by rotating disk electrode

Hydrodynamic electrochemical studies using the rotating disk electrode (RDE) were carried out for the purpose of determining important kinetics parameters that help not only in the study of stability and electrochemical behavior, but also to understand the kinetic mechanism of charge transfer in aqueous solution for binuclear and tetranuclear oxo-manganese complexes.

Fig. 3 shows the voltammetric profile of RDE for complexes in aqueous solution with rotation rate of 100 to 5000 rpm. Analyzing

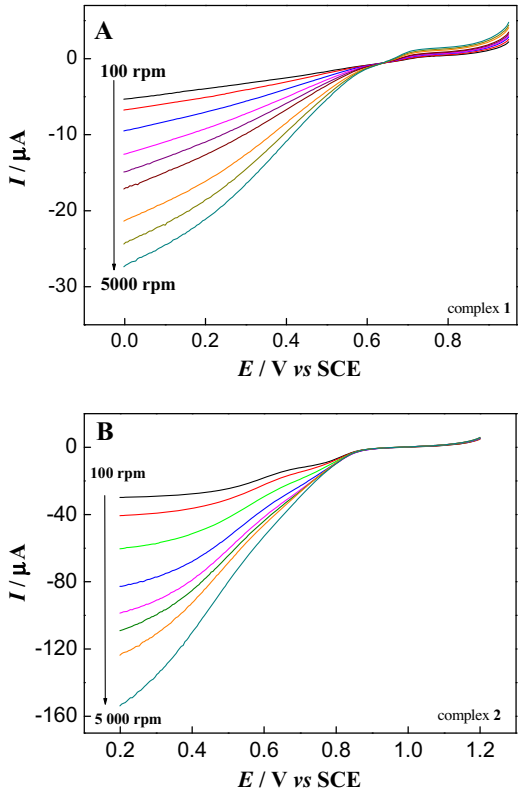

Fig. 3. Linear voltammogram recorded with rotating disk electrode (RDE) for (A) binuclear oxo-manganese complex (0–1.0 V vs. SCE) and (B) tetranuclear oxo-manganese complex (0.2–1.2 V vs. SCE) in 0.5 mol L^{-1} $NaNO_3$ containing 1 mmol L^{-1} of respective complex. Rotation rates at 100, 200, 500, 1000, 1500, 2000, 3000, 4000 and 5000 rpm. $v = 25$ mV s^{-1}.

the voltammogram profiles, the mass transport limited current plateau is shifted further away from the apparent redox potential indicative of a slow kinetics [30]. Stated another way, when a redox reaction is sluggish, a larger overpotential must be applied to the electrode to overcome the sluggish kinetics and reach the mass transport limited current.

Fig. 3B shows that the first limiting current plateau is influenced by rotation rate, indicating that the limiting current value is affected by the mixed control region of the primary reaction and from the current generated by the secondary reaction. The limiting current region can be affected by factors such as the secondary reaction changes in the concentration of the electroactive species, electronic transfer effects when the mixed control region extends towards the limiting current region, as in the case of slow and irreversible reactions [31]. The irreversibility of the system demonstrates that in aqueous solution the complex has higher stability with $Mn^{(IV)}O_2Mn^{(IV)}$ and $Mn^{(IV)}O_2Mn^{(IV)}OMn^{(IV)}O_2Mn^{(IV)}$, which is reduced irreversibly to $Mn^{(IV)}O_2Mn^{(III)}$ and $Mn^{(IV)}O_2Mn^{(III)}OMn^{(III)}$-$O_2Mn^{(IV)}$, respectively for binuclear and tetranuclear. The ligand field of di-μ-oxo coordination compounds is defined on *xy* plane, directing the Mn atoms on the *z* axis of the oxo-Mn-oxo plane. The energy variation observed in the dimers is associated with the loss of degeneration of orbitals present in the di-μ-oxo bond [32]. The ligand field energy is higher to Mn^{IV} than Mn^{III} ions, which can be ascribed to electron distribution and stability of these orbitals. The Mn^{IV} ion shows the d^3 system, and thus, the *d*–*d* electron transition occurs in $t_{2g}^3 \rightarrow t_{2g}^2\, e_g^1$ orbitals. On the other hand, the Mn^{III} ions show the d^4 system, where the tetragonal distortion stabilizes the complex, distributing the electrons to occupied and unoccupied t_{2g} and e_g orbitals. The *d*–*d* electron transition occurs in $t_{2g}^3\, e_g^1 \rightarrow t_g^2\, e_g^2$. Thus, this structure with Mn^{III} centers can suffer the *Jahn Teller* effect in the *z* axis, with ligand field influence [2,32] proving the instability for complexes $Mn^{III}Mn^{III}$ with possible breakdown of the complex. In this way, the structure containing Mn^{IV} centers shows higher stability, because these complexes don't have *Jahn–Teller* distortion.

At low rotation rates, two redox processes can be observed for tetranuclear complex, which were confirmed by the first derivative (Fig. 4), where the potential peak are similar to observed in the cyclic voltammogram of the tetranuclear oxo-manganese complex (Fig. 1B). However, the first derivative at voltammetric curve was obtained at 5000 rpm a shift of the potential peak to a more negative value and a great increase in the first process was observed. Thus, for low rotation rate, only the electrochemical step can be observed due to a double layer effect, where the reduction process occurs separately for binuclear (process II) and tetranuclear (process I) oxo-manganese complexes (Scheme 1).

The μ-oxo-bridge present in tetranuclear complex structures provides a fast electron transition between metal centers due to stabilization of $dx^2 - y^2$ orbitals by the oxygen bond, which contributes to reduction process that occurs in potential more negative than to binuclear oxo-manganese complex. For binuclear

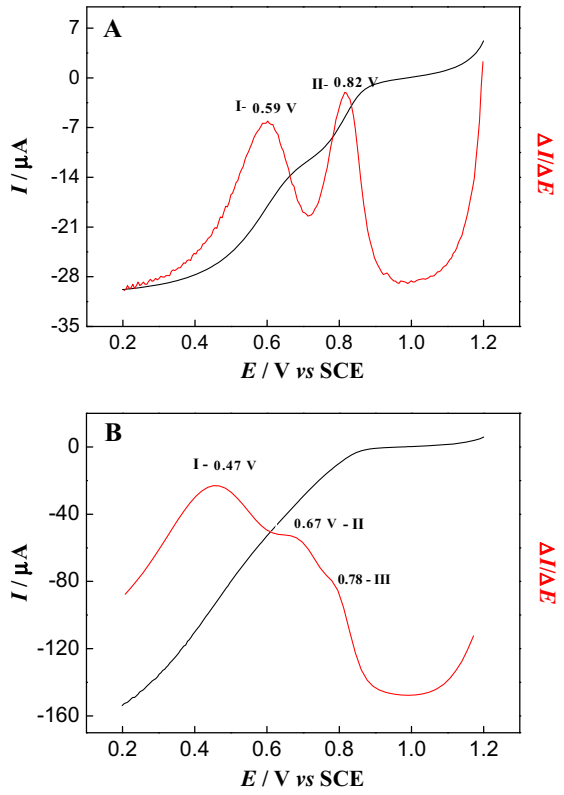

Fig. 4. RDE voltammogram for tetranuclear oxo-manganese complex obtained from (A) 100 rpm and (B) 5000 rpm, with the first derivative curve illustrated in detail.

complex, the $dx^2 - y^2$ orbitals are stabilized by *aqua* ligands through a coordination bond, which causes a displacement of potential reduction to a more positive potential. This way, it may be influenced by the double layer. Comparing the complexes, the coordination bond promotes a higher stabilization of $dx^2 - y^2$ orbitals for Mn^{IV} centers, when the reduction for Mn^{III} is difficult. Therefore, the process observed at 0.59 V (100 rpm) and 0.47 V versus SCE (5000 rpm) can be ascribed to tetranuclear complex, and the process observed at 0.82 V (100 rpm) and 0.78 V versus SCE (5000 rpm) can be ascribed to the behavior of the binuclear complex.

This behavior proved the presence of binuclear and tetranuclear complex in dimerization equilibrium; which was also observed in the voltammetric study. Thus, the calculation of kinetics parameters was done considering processes I and II for binuclear complex. However, for higher rotation values the shift of potential values can be related to a chemical step, since that a compression of the Nernst diffusion layer occurs by rotating the electrode, the dimerization process decrease the reduction of the binuclear species and increase of the tetranuclear species. These results prove the observation realized by studies in cyclic voltammetry, where in solution for tetranuclear oxo-manganese complex, there is the possibility of binuclear oxo-manganese complex in equilibrium by dimerization process (Scheme 2). The process observed at 0.67 mV (peak II) can be ascribed to an intermediate complex, where the hydroxyl group is still in the complex structure, as can be observed in Scheme 3.

For an irreversible system, the rate constant of the electron transfer (k_e) increases with increment of potential applied on the electrode to reach a plateau of limiting current [33]. The magnitude of transfer constant is directly dependent of the potential applied and standard rate constant (k_0). Another important parameter in irreversible system is the nonexistence of the equilibrium of species on the surface and hence the inapplicability of the Nernst equation with redox potential as a function of the rotation rate of electrode. This can be ascribed to the potential of half-wave ($E_{1/2}$) being a function of mass transfer coefficient (k_d) in an irreversible system [31]. The k_d describes the diffusion rate within the diffusion layer, where it is influenced by the thickness of the diffusion layer, which is controlled by rotation variation (convection). For irreversible systems, the magnitude of standard rate constant is smaller than the mass transfer coefficient ($k_0 \ll k_d$).

Applying the data from Fig. 3 in the Heyrovský–Ilkovic equation (Eq. (1)) for irreversible systems, a linear relation to $\log(I_L - I/I)$ versus $E_{applied}$ was obtained.

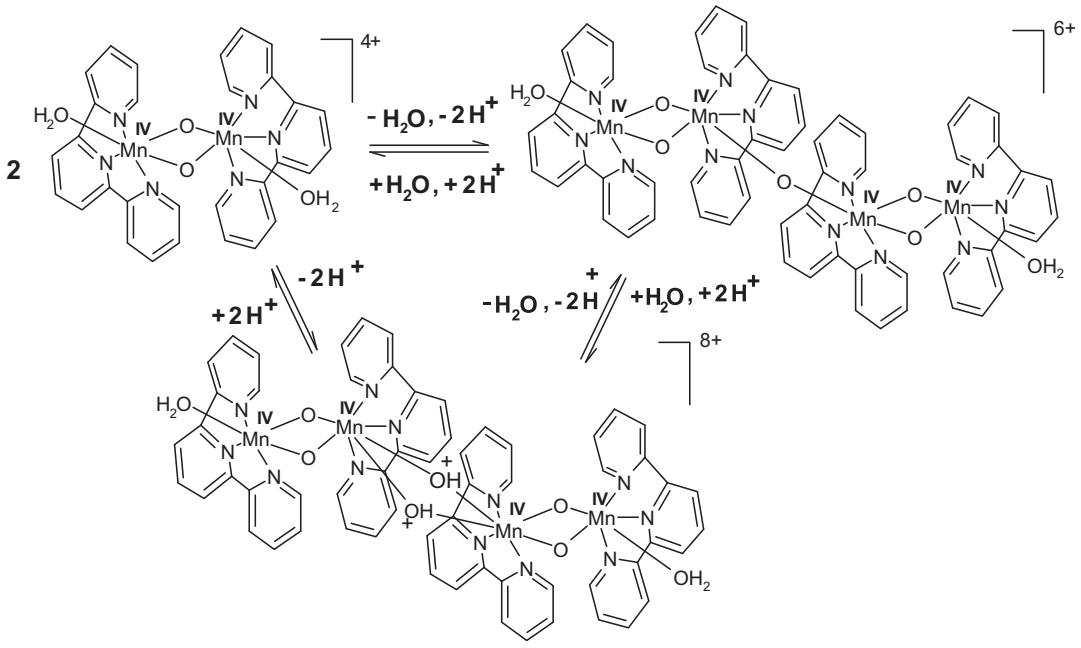

Scheme 3. Representation of chemical step with formation of the intermediate complex.

$$E = E_{1/2}^{irr} - \frac{RT}{\alpha_c nF} \ln \frac{I_L - I}{I} \quad (1)$$

where α_c is the cathodic charge transfer coefficient, n the electron number, I current observed, I_L, limit current for fixed potential and $E_{1/2}$ the wave-half potential. The slope of the relation can be represented by:

$$\text{slope} = -\frac{2,303RT}{\alpha_c nF} \quad (2)$$

The cathodic charge transfer coefficient and wave-half potential were determined according to Eq. (2). The $E_{1/2}$ values for each rotation rate utilized are listed in Table 1.

However, for $\alpha_c n$ values, a different behavior can be observed (Fig. 5) for both complexes studied. A decrease in $\alpha_c n$ with increase in rotation rate for tetranuclear complex (process I) and an increase of the $\alpha_c n$ with increase in rotation rate for process II was observed, and for binuclear complex as well as. Accordingly, process II can be ascribed to the behavior of the binuclear complex.

The kinetic current can be analyzed by Koutecky–Levich equation, where the current observed (I), for the fixed potential, in relation to rotation rate of the electrode (ω) is:

$$\frac{1}{I} = \frac{1}{I_k} + \frac{1}{I_L} \quad (3)$$

where I_k is the kinetic current (absence of any mass transfer effect) and I_L the limit diffusion current, which is related to rotation rate (ω) by the Levich equation [30,33]:

Table 1
Wave-half potential ($E_{1/2}$) vs. rotation rate (ω) for binuclear oxo-manganese and tetranuclear oxo-manganese complexes.

ω		$E_{1/2}$ (mV vs. SCE)		
rpm	rad s^{-1}	Binuclear oxo-manganese	Tetranuclear oxo-manganese	
			(Process I)	(Process II)
100	10.472	418	646	681
200	20.944	406	639	673
500	52.360	391	630	662
1000	104.72	380	623	652
1500	157.08	376	616	647
2000	209.44	375	611	643
3000	314.16	375	603	637
5000	523.60	375	596	634

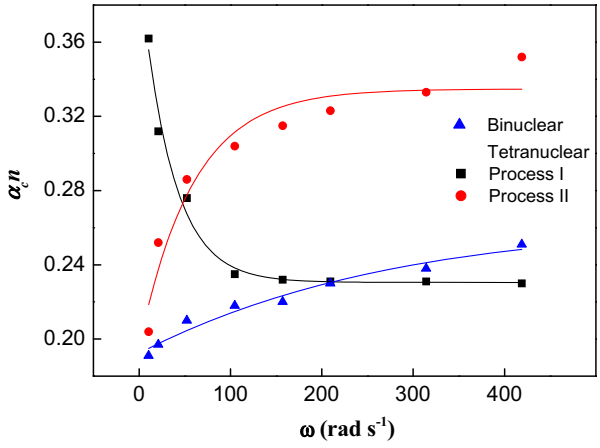

Fig. 5. Charge transfer coefficient ($\alpha_c n$) with rotation rate (10.472–523.60 rad s^{-1}) obtained by Eq. (6). Charge transfer coefficient for binuclear complex and tetranuclear complex (process I and II), respectively.

$$I_L = 0.62nFAC_0D^{2/3}v^{-1/6}\omega^{1/2} \quad (4)$$

where A is electrode area (0.072 cm^2), D diffusion coefficient (cm^2 - s^{-1}), ω rotation rate (rad s^{-1}), v kinetic viscosity of the solvent (9.025×10^{-3} cm^2 s^{-1} at 25 °C), C_0 complex concentration in solution, F Faraday constant (96,485.3 C/mol e^-) and n number of electrons involved in transfer reaction. By selecting the potential range between the limiting current and the linear region close to the wave-half potential, the plot of $1/I$ versus $1/\omega^{1/2}$ (Koutecky–Levich plot) was obtained. The kinetic current was obtained according to the linear coefficient of the Koutecky–Levich plot, and the values of the apparent rate constant (k'_e) can then be obtained by the equation:

$$I_k = nFAk'_eC \quad (5)$$

In the linear region of the voltammogram (Tafel region), the current density depends exponentially on the potential [33]. This way, considering that the system shows only oxidized species within the solution (where only reduction occurs), we have the relation:

$$k'_e = k_0 \exp[-\alpha_c nF(E - E^{\theta})/RT]$$
$$\log k'_e = \log k_0 - \frac{\alpha_c nF}{RT}E \quad (6)$$

where k_0 is the standard rate constant. Thus, applying log k'_e versus applied potential (Fig. 6), the k_0 and $n\alpha_c$ values were calculated by the linear coefficient and slope, respectively.

The k_0 value for binuclear oxo-manganese complex was 15.42 cm s^{-1}, and for tetranuclear oxo-manganese complex were 1.83×10^{-4} cm s^{-1} and 0.076 cm s^{-1} for process I and II, respectively. The $n\alpha_c$ values of 0.25, 0.05 and 0.15 were determined for binuclear complex and process I and II of the tetranuclear complex, respectively. The values obtained from Eq. (6) are in accordance with results obtained by Heyrovský–Ilkovic. The standard rate constant is a measure of the kinetic facility of a redox couple. A system with large k_0 will achieve equilibrium on a short time scale, but a system with small k_0 will be sluggish [28]. Thus, for binuclear oxo-manganese complex and process II of the tetranuclear oxo-manganese complex, the dimerization equilibrium is favored with increase of the rotation rate. However, the k_0 for process I show that equilibrium is sluggish. Therefore, the redox process is not influenced by the rotation rate.

The diffusion coefficient was calculated by the Levich equation (Eq. (4)). Thus, by the limiting currents for binuclear complex at 0.10 V, for tetranuclear complex at 0.44 V and 0.77 V versus SCE for process I and II, respectively, were plotted for different rotation rate values. The Levich plot shows linearity with I_L versus $\omega^{1/2}$, where the diffusion coefficient of 1.16×10^{-6}, 1.29×10^{-5} and 2.38×10^{-4} cm^2 s^{-1}, for binuclear complex and tetranuclear complex (process I and II), respectively, was obtained by slope. This behavior can be ascribed to dimerization process frequently observed for this complex. The binuclear oxo-manganese complex showed a low rate of charge transfer, while the tetranuclear oxo-manganese complex showed a higher rate of charge transfer, which can be ascribed not only to overlap of orbitals $d\pi$–π, but also to the presence of a mono-μ-oxo bridge, which minimizes the *Jahn Teller* effect during the reduction process. The overlap of orbitals $d\pi$–π favored the multi-electron transfer, observed for polynuclear complex. Thus, the binuclear oxo-manganese complex with terpyridine as ligand tends to form tetranuclear species in aqueous solution.

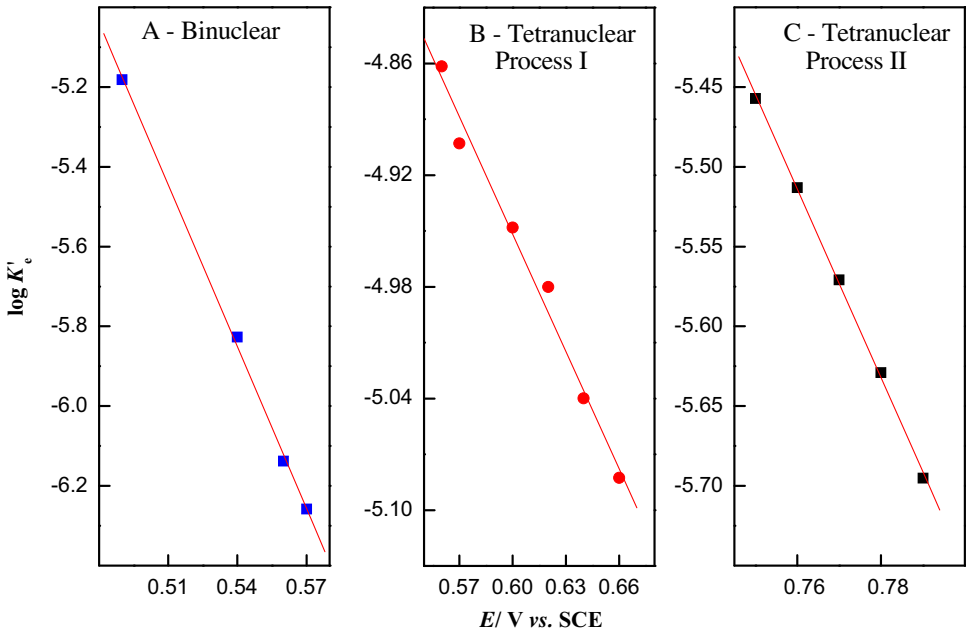

Fig. 6. Dependence of k'_e on potential applied in Tafel range to determination of the k_0 and $\alpha_c n$ constant for (A) binuclear oxo-manganese complex, (B) process I and (C) process II of tetranuclear oxo-manganese complex.

4. Conclusions

In summary, the hydrodynamic study with RDE determined the stability of binuclear and tetranuclear oxo-manganese complexes in aqueous solution, which showed a great stability for systems with Mn^{IV} centers (Supporting material). The stability and kinetic behavior are directly related to a μ-oxo bridge, where the μ-oxo-bridge provides a fast electron transition between metal centers due to stabilization of $dx^2 - y^2$ orbitals by oxygen bond. On the other hand, when the $dx^2 - y^2$ orbitals are stabilized by *aqua* ligands by coordination bond, a displacement of oxidation potential to more positive potential was observed. The kinetic parameters were dependent on the potential applied and rotation rate, where the shift of the potential to more negative values with increase in rotation rate can be ascribed to the chemical step. The chemical step involves the dimerization process of the binuclear oxo-manganese complex to tetranuclear oxo-manganeses complex.

Acknowledgments

The authors are thankful to CNPq (474367/2004-5) by research support. The scholarships granted by FAPESP (2009/11079-1) and (2010/12524-6) to C.S. Martin is gratefully acknowledged. SJT is also thanked.

Appendix A. Supplementary material

Supplementary data associated with this article can be found, in the online version, at http://dx.doi.org/10.1016/j.ica.2014.10.009.

References

[1] C. Baffert, S. Romain, A. Richardot, J.C. Lepretre, B. Lefebvre, A. Deronzier, M.N. Collomb, J. Am. Chem. Soc. 127 (2005) 13694.
[2] H.Y. Chen, J.W. Faller, R.H. Crabtree, G.W. Brudvig, J. Am. Chem. Soc. 126 (2004) 7345.
[3] M.N. Collomb, A. Deronzier, A. Richardot, J. Pecaut, New J. Chem. 23 (1999) 351.
[4] J. Limburg, J.S. Vrettos, H.Y. Chen, J.C. de Paula, R.H. Crabtree, G.W. Brudvig, J. Am. Chem. Soc. 123 (2001) 423.
[5] J. Limburg, G.W. Brudvig, R.H. Crabtree, J. Am. Chem. Soc. 119 (1997) 2761.
[6] V.L. Pecoraro, Manganese Redox Enzymes, VCH, New York, NY, 1992.
[7] D. Srinivas, S. Sivasanker, Catal. Surv. Asia 7 (2003) 121.
[8] K. Ozette, P. Battioni, P. Leduc, J.F. Bartoli, D. Mansuy, Inorg. Chim. Acta 272 (1998) 4.
[9] N.W.J. Kamp, J.R.L. Smith, J. Mol. Catal. A: Chem. 113 (1996) 131.
[10] R. Ganesan, B. Viswanathan, J. Mol. Catal. A: Chem. 223 (2004) 21.
[11] T. Tzedakis, Y. Benzada, M. Comtat, Ind. Eng. Chem. Res. 40 (2001) 3435.
[12] J.J. Dannacher, J. Mol. Catal. A: Chem. 251 (2006) 159.
[13] R. Manchanda, G.W. Brudvig, R.H. Crabtree, Coord. Chem. Rev. 144 (1995) 1.
[14] W. Ruttinger, G.C. Dismukes, Chem. Rev. 97 (1997) 1.
[15] V.K. Yachandra, K. Sauer, M.P. Klein, Chem. Rev. 96 (1996) 2927.
[16] F.M. Ashmawy, C.A. Mcauliffe, R.V. Parish, J. Tames, Dalton Trans. (1985) 1391.
[17] M.C. Ghosh, J.W. Reed, R.N. Bose, E.S. Gould, Inorg. Chem. 33 (1994) 73.
[18] M.N.C. Dunand-Sauthier, A. Deronzier, X. Pradon, J. Am. Chem. Soc. 119 (1997) 3173.
[19] M.M. Najafpour, A.N. Moghaddam, H. Dau, I. Zaharieva, J. Am. Chem. Soc. 136 (2014) 7245.
[20] M. Wiechen, H.M. Berends, P. Kurz, Dalton Trans. 41 (2012) 21.
[21] S.R. Cooper, M. Calvin, J. Am. Chem. Soc. 99 (1977) 6623.
[22] J.E. Sarneski, M. Didiuk, H.H. Thorp, R.H. Crabtree, G.W. Brudvig, J.W. Faller, G.K. Schulte, Inorg. Chem. 30 (1991) 2833.
[23] R.A. Binstead, M.E. Mcguire, A. Dovletoglou, W.K. Seok, L.E. Roecker, T.J. Meyer, J. Am. Chem. Soc. 114 (1992) 173.
[24] E. Adams, L. Frank, Annu. Rev. Biochem. 49 (1980) 1005.
[25] R. Ramaraj, A. Kira, M. Kaneko, Angew. Chem. 25 (1986) 825.
[26] M.N.C. Dunand-Sauthier, A. Deronzier, A. Piron, J. Electroanal. Chem. 463 (1999) 119.
[27] M.N.C. Dunand-Sauthier, A. Deronzier, A. Piron, X. Pradon, S. Menage, J. Am. Chem. Soc. 120 (1998) 5373.
[28] C.S. Martin, M.F.S. Teixeira, Dalton Trans. 40 (2011) 7133.
[29] D.R. Gamelin, M.L. Kirk, T.L. Stemmler, S. Pal, W.H. Armstrong, J.E. Pennerhahn, E.I. Solomon, J. Am. Chem. Soc. 116 (1994) 2392.
[30] C.M.A. Brett, A.M.O. Brett, Electrochemistry: Principles, Methods, and Applications, Oxford University Press, Oxford; New York, 1993.
[31] A.J. Bard, L.R. Faulkner, Electrochemical Methods: Fundamentals and Applications, Wiley, New York, 2001.
[32] B. Albela, G. Chottard, J.J. Girerd, J. Biol. Inorg. Chem. 6 (2001) 430.
[33] C. Ponce-de-Leon, C.T.J. Low, G. Kear, F.C. Walsh, J. Appl. Electrochem. 37 (2007) 1261.